2012 American Control Conference
Fairmont Queen Elizabeth, Montréal, Canada
June 27-June 29, 2012

Power Optimization for Photovoltaic Micro-Converters using Multivariable Gradient-Based Extremum-Seeking

Azad Ghaffari, Sridhar Seshagiri, and Miroslav Krstić

***Abstract*— It is well-known that *distributed architectures* such as micro-converters and micro-inverters for photovoltaic (PV) systems can recover between 10%-30% of annual performance loss or more that is caused by partial shading and/or module mismatch. In this work, we present a novel multivariable gradient-based extremum-seeking (ES) design to extract maximum power from an arbitrary micro-converter configuration of PV modules, that includes cascade and parallel connections. Conventional maximum power point tracking (MPPT) schemes for micro-converters (where each PV module is coupled to its own DC-DC converter) employ a decentralized control, with one peak seeking scheme per each PV module, thereby requiring one control loop and two sensors per module (one each for current and voltage). By contrast, the scheme that we present employs a single control loop with just two sensors, one for the overall array output current and the other one for the DC bus voltage. This centralized design provides more flexibility in tuning the parameters of the controller, and also takes into account interactions between PV modules. The computational effort of our design is not higher than that of the conventional scheme, and simulation results using Simulink's SimPowerSystems toolbox show that our proposed design outperforms the conventional one. Thus, our proposed design offers two benefits: (i) the balance-of-system (BOS) cost reduction as a result of the significantly lower number of sensors, and (ii) improved performance, both contributing towards reduced average cost/watt, and enhancing the economic viability of solar.**

I. Introduction

a) Motivation: Maximum power point tracking (MPPT) is a technique for maximizing the energy extracted from PV modules. Over the years, many MPPT methods have been developed and implemented [2], [3], [5], [6], [7], [8], [9], [11], [12], [13], [14], [15], [16], [17], [18]. These methods vary in complexity, convergence speed, cost, range of effectiveness, implementation hardware, popularity, etc. Comprehensive comparative analyses of currently available techniques can be found in [6], [7], [8].

Extremum-seeking (ES) is a non-model-based real-time optimization algorithm [1], [10], [20], [21] for systems with unknown dynamics that has been applied to a wide range of technical applications, including MPPT in PV systems [2], [3], [11], [12], [14]. It offers the advantages of fast convergence and guaranteed stability over a range of environmental conditions, and yet is simple to implement, and hence very cost effective in terms of processing/hardware requirements.

With the exception of [2], all existing work on ES applies the technique to PV systems whose cells receive the same irradiance level, i.e., have unimodal power characteristics. Recent works (for example, [5]) concentrate on designing MPPT methods to track multiple peaks (non-unimodal power) under rapidly changing irradiance conditions, and the issues of partial shading and module mismatch. These studies have led to a growing interest in distributed architectures (also referred to as distributed power electronics), such as micro-converters (distributed DC-DC converters) and micro-inverters (distributed DC-AC converters) [4]. While [2] deals with ES design for micro-converters (one DC-DC converter for each module), it employs a scalar ES loop for each PV module. Two problems arise here. First, this scheme requires two sensors per module, current and voltage, which increases the levelized energy cost. Second, the coupling effect between PV modules is not addressed by this decentralized control. Our current work shows that employing a multivariable MPPT algorithm instead of separate scalar ones solves these problems.

To the best of our knowledge, there are a limited number of multivariable MPPT schemes described in the literature, among which we refer the reader to [13], [17], [18]. The last of these references [18] uses a multivariable version of the popular Perturb and Observe (P&O) algorithm. Unlike scalar designs which require one current sensor for each module, the algorithm only requires a single current sensor on the DC bus. The operating point of the DC/DC converters are perturbed asynchronously, to minimize the possibility of converter interaction having a detrimental effect on the other modules. Closely related to [18] is the work in [17], where "extra variables" are employed in the classical P&O algorithm to overcome the limitation of scalar designs, which the authors say fail when the feasibility region is nonconvex. It is unclear how [17] compares with distributed architectures, with respect to power loss recovery in the case of module mismatch. Reference [13] uses Particle Swarm Optimization (PSO), which is an algorithm that employs multiple agents to "search" for the peak power. The paper does not describe the specific criteria used to select the number of agents and parameters of the PSO, nor the conditions on the voltage and power boundary limits to stop the algorithm at Maximum Power Point (MPP). Also, in a PV system with a higher number of PV modules, the process of reinitialization and the tracking performance depend strongly on variable conditions like environmental factors, the nature of the PV modules, and

Azad Ghaffari is with Joint–Doctoral Programs (Aerospace and Mechanical) between San Diego State University and University of California at San Diego, La Jolla, CA 92093-0411, USA, aghaffar@ucsd.edu.

Sridhar Seshagiri is with Department of Electrical and Computer Engineering, San Diego State University, San Diego, CA 92182-1309, USA, seshagir@engineering.sdsu.edu.

Miroslav Krstić is with Department of Mechanical and Aerospace Engineering, University of California, San Diego, La Jolla, CA 92093-0411, USA, krstic@ucsd.edu.

978-1-4577-1096-4/12/$26.00 ©2012 AACC

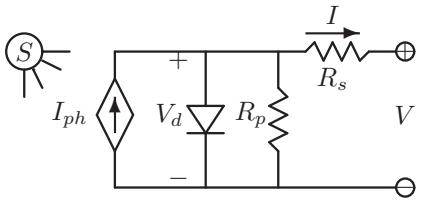

Fig. 1. Equivalent circuit of a PV cell.

the shading area. The authors claim that the required number of sensors are reduced to two, but to compute the pulse duration, the output voltage of each boost converter needs to be monitored by a separate sensor. The method also has an adaptation time of the order of 1-2 seconds. By contrast, the response time in ES-based designs is much smaller, of the order of 0.1 seconds.

b) Our contribution: We present a multivariable gradient-based ES schemes with the following features: (1) It is applied to micro-converter systems, and hence deals with the case of non-unimodal power characteristics, and deals specifically with the issue of module mismatch (for example, possibly different irradiance levels as a result of partially shaded conditions). (2) The use of the non-model-based ES technique makes the design robust to partial knowledge of the system parameters and operating conditions. (3) As opposed to scalar designs, our multivariable design only requires 2 sensors in all, for the overall PV system current, and the DC bus voltage. This is a significant reduction in hardware cost. (4) Moreover, interactions between PV modules are inherently part of the multivariable design, and hence the transient performance is less-sensitive to environmental variable variations than a corresponding scalar design. (5) The computational burden is of the same order as a scalar design, but with a slightly faster transient response than scalar ES designs, and significantly faster than non-ES based designs such as [13].

c) Organization: The rest of this paper is organized as follows: The mathematical model of a PV module, along with a discussion of the DC/DC converter power electronics, is presented in Section II. Section III introduces the scalar gradient-based ES scheme, presented for clarity for the case of a single module first, followed by how this is conventionally extended to the distributed micro-converter case. Our proposed multivariable gradient-based ES is presented and discussed in Section IV, along with some simulation results in Section V, and a summary of our design and some concluding remarks in Section VI.

II. Photovoltaic Modules and Power Extraction

Our design and analysis are based on the standard PV cell model described for example in [19], and shown schematically in Fig. 1. The PV cell is modeled as an ideal current source of value I_{ph} in parallel with an ideal diode with voltage V_d. Electrical losses and contactor resistance are accounted for by the inclusion of the parallel and series resistances R_s and R_p respectively. The amount of generated current I_{ph} is dependent on the solar irradiance S and the

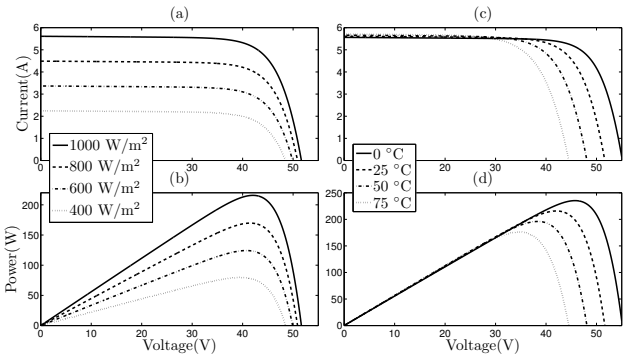

Fig. 2. Characteristic (a) I–V and (b) P–V for varying irradiance, T=25°C. Characteristic (c) I–V and (d) P–V for varying temperature, S=1000W/m^2.

temperature T through the following equation

$$I_{ph} = \left(I_{ph}^r + k_i(T - T_r)\right)\left(\frac{S}{1000}\right), \tag{1}$$

where I_{ph}^r is a reference short-circuit current, T_r a reference temperature, and k_i the short-circuit temperature coefficient. The diode models the effect of the semiconductor material and its $I-V$ characteristics are given by

$$I_d = I_0\left(\exp\left(\frac{V_d}{V_t}\right) - 1\right), \tag{2}$$

$$I_0 = I_0^r\left(\frac{T}{T_r}\right)^3 \exp\left[\frac{qE_g}{Ak}\left(\frac{1}{T_r} - \frac{1}{T}\right)\right], V_t = \left(\frac{AkT}{q}\right) \tag{3}$$

where I_0^r, E_g and A are respectively the diode reference reverse saturation current, the semiconductor bandgap energy, and an ideality factor, all three being cell material/construction dependent, V_t is the thermal cell voltage, and $k = 1.38 \times 10^{-23}$ J/°K and $q = 1.6 \times 10^{-19}$ C are Boltzman's constant and the charge on an electron respectively. The cell model described by the above equations along with KCL/KVL: $I = I_{ph} - I_d - V_d/R_p$, $V_d = V + IR_s$, is then scaled to represent a PV module by considering n_s cells in series (each having cell voltage V_t), so that the terminal $I-V$ relationship for the PV module is given by

$$I = I_{ph} - I_0\left[\exp\left(\frac{\frac{V}{n_s} + IR_s}{V_t}\right) - 1\right] - \left[\frac{(\frac{V}{n_s} + IR_s)}{R_p}\right]. \tag{4}$$

For the sake of model development and performing simulations (done using the SimPowerSystems toolbox of Simulink), we pick the PV module 215N from Sanyo, with the following numerical values derived from the manufacturer's datasheet: $E_g = 1.16$ eV, $A = 1.81$, $I_0^r = 1.13 \times 10^{-6}$ A, $I_{ph}^r = 5.61$ A, $k_i = 1.96$ mA/°K, $T_r = 298.15$ °K, $R_s = 2.48$ mΩ, $R_p = 8.7$ Ω, and the number of PV cells connected in series is $n_s = 72$. The resulting $I-V$ and $P-V$ curves are shown in Fig. 2.

As is clear from Fig. 2(b,d), the power-voltage (P-V) characteristic has a unique but (T, S) dependent peak (V^*, P^*). It is the job of the MPPT algorithm to automatically track this peak. In many grid-tied PV systems (including our current work), this is done by means of a separate DC/DC power

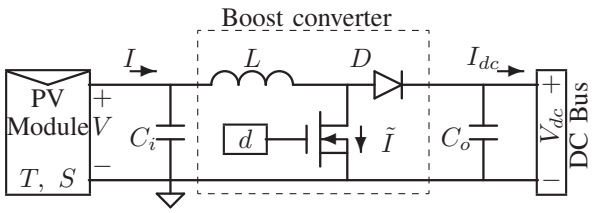

Fig. 3. PV module supplying power to a DC bus via a DC-DC boost converter.

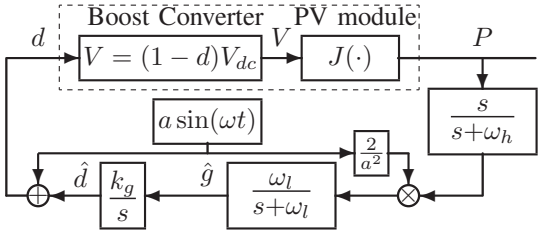

Fig. 4. Scalar extremum seeking for MPPT of a PV module.

electronics stage that serves two functions: (i) regulating the output DC voltage at a (near) constant value, and (ii) extracting maximum power by forcing the PV module output V to equal V^*. Fig. 3 shows this setup for a DC/DC boost converter stage, whose output voltage is maintained constant as $V_{\rm dc}$. The ratio between the input voltage V and output voltage V_{dc} can be controlled by changing the duty cycle of the transistor switch, which serves as the control input d. Under the assumption that the boost converter is working in Continuous Current Mode (CCM), and that the switching Pulse Width Modulation (PWM) frequency f_c is significantly higher than the bandwidth of the control loop, the boost converter input-output voltage relationship is given by the following (averaged) relation:

$$V = V_{\rm dc}(1-d), \tag{5}$$

From (4), (5) and Fig. 2(b,d), it follows that at the MPP (V^*,P^*), the power $P = IV = f(V)V \stackrel{\rm def}{=} J(V)$, satisfies

$$g = \frac{\partial J}{\partial V}(V^*) = 0 \tag{6}$$

$$h = \frac{\partial^2 J}{\partial V^2}(V^*) < 0. \tag{7}$$

Also we have $\partial V/\partial d = -V_{dc}$ then

$$\bar{g} = \frac{\partial J}{\partial d}(d^*) = -V_{dc} g = 0 \tag{8}$$

$$\bar{h} = \frac{\partial^2 J}{\partial d^2}(d^*) = V_{dc}^2 h < 0. \tag{9}$$

Many MPPT techniques, including the classical perturb-and-observe (P&O) class of methods, and extremum-seeking (ES) techniques, are based on detecting the sign of the power gradient. The next section discusses scalar gradient-based ES in more detail.

III. Scalar Gradient-Based Extremum Seeking

Several authors have considered to use scalar gradient-based ES for the MPPT problem [2], [3], [11], [12], [14]. Fig. 4 shows the basic setup of the scheme for the case of a single PV module, and its principal features have been explained fairly clearly in the aforementioned references, but we reproduce them here for the sake of completeness/clarity.

The injection of the small periodic perturbation $a\sin(\omega t)$ to the estimate $\hat{d}$ of the optimal pulse duration d^* results in a periodic power output P, whose DC component is removed by the wash-out filter $s/(s+\omega_h)$, with the resultant signal being in phase or out of phase with the perturbation according to whether $\hat{d}$ is greater than or less than d^* respectively. Multiplication of this signal by $2\sin(\omega t)/a$ and extracting the DC component of the product using the low-pass filter $\omega_l/(s+\omega_l)$ results in an estimate of the gradient of the cost function. Defining $\tilde{d} = \hat{d} - d^*$, and expanding P about its optimal value and using (6), (7), we see that the ES design of Fig. 4 implements the gradient update law

$$\dot{\hat{d}} = k_g \bar{h}\tilde{d} = k_g V_{dc}^2 h \tilde{d}, \tag{10}$$

where h is the Hessian. Design guidelines for selecting the parameters a, ω, ω_h, ω_l, and k_g can be found in [10], but are mentioned here for sake of completeness. The frequency ω must be chosen small enough to ensure that the plant dynamics appear as a static nonlinearity from the viewpoint of the ES loop, and the filter frequencies chosen such that $\omega_h < \omega_l \ll \omega$, so that the low pass filter attenuates the perturbation frequency, whereas the high-pass filter does not. The adaptation gain k_g and the amplitude a of the probing signal need to be "sufficiently small". Define

$$\omega_l = \omega\delta\omega_l' \tag{11}$$

$$\omega_h = \omega\delta\omega_h' \tag{12}$$

$$k_g = \omega\delta k_g', \tag{13}$$

where ω and δ are small positive real numbers, and ω_h', ω_l' and k_g' are $O(1)$ positive real parameters. The analysis of [10] shows that for sufficiently small ω, a, and δ, the output P converges to an $O(\omega+\delta+a)$-neighborhood of the MPP P^*.

The above design for a single module can be extended to the PV system shown in Fig. 5, that has m parallel strings, with each string having n modules in cascade (series). Since irradiance (and temperature to a lower extent) may vary between the modules, the peak power is not necessarily the same for all of them. This "module mismatch" therefore results in maximum powers for string architectures that are lower than the sum of the individual maximum powers of the modules, which in turn has led to the use of micro-converters, where each module is coupled with its own DC-DC converter. Micro-converter architectures can recover between 10%-30% of annual performance loss caused due to module mismatch. The conventional way to implement the MPPT algorithm in micro-converters is to simply extend the preceding (scalar) MPPT design to each PV module, as shown in Fig. 6 for one string. In each string we therefore have n separate control loops, with no consideration to the

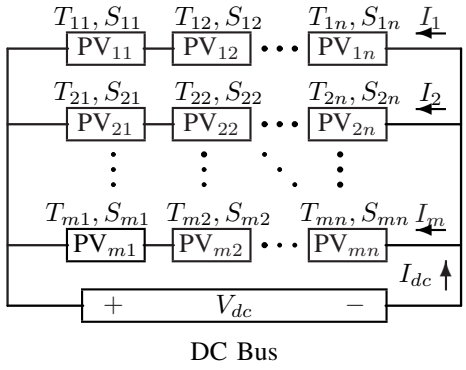

Fig. 5. PV system including m parallel strings. Each string has n PV modules in cascade

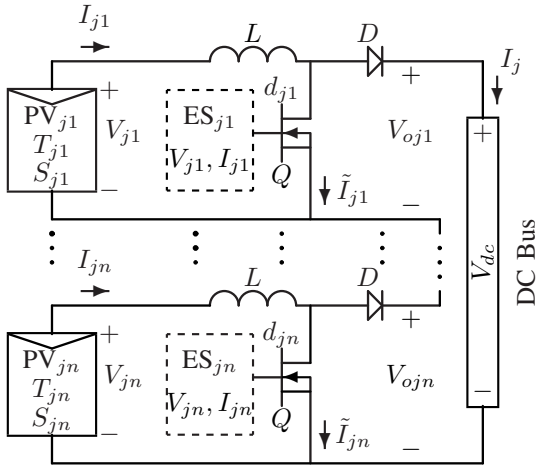

Fig. 6. Decentralized MPPT for string j, where $j = 1, 2, \cdots, m$. One scalar ES loop is used for each PV module.

interaction between the series modules. We also still have two sensors per module, that measure the module voltage and current. The multivariable control algorithm that we present in the next section allevaites both these issues; on the one hand, it considers the interaction between modules, resulting in better performance, and in addition, uses just two sensors for the overall system, resulting in substantial hardware reduction cost. The details of the actual design are presented in the next section.

IV. Multivariable Gradient-Based Extremum Seeking

A block schematic of our proposed multivariable gradient-based ES is shown in Fig. 7. As is clear from the schematic, the design employs just one ES loop with two sensors for the overall system, one each for the DC bus voltage V_{dc} and the overall current I_{dc}.

Fig. 8 shows the multivariable extension of the ES design that is described by Fig. 4, and its principal features are essentially the same as discussed in Section III. In particular, the design derives an estimate $\hat{G}$ of the gradient vector by adding a probing signal to the estimate $\hat{D} = [\hat{d}_{11}\ \hat{d}_{12}\ \cdots\ \hat{d}_{mn}]^T$ of the pulse duration vector (of all the

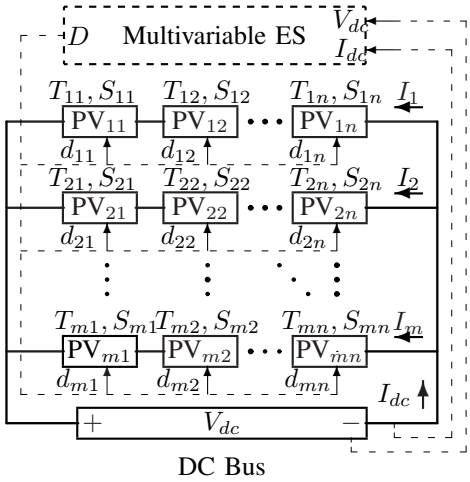

Fig. 7. Our proposed centralized MPPT for PV system, just one multivariable ES loop is employed for all PV modules.

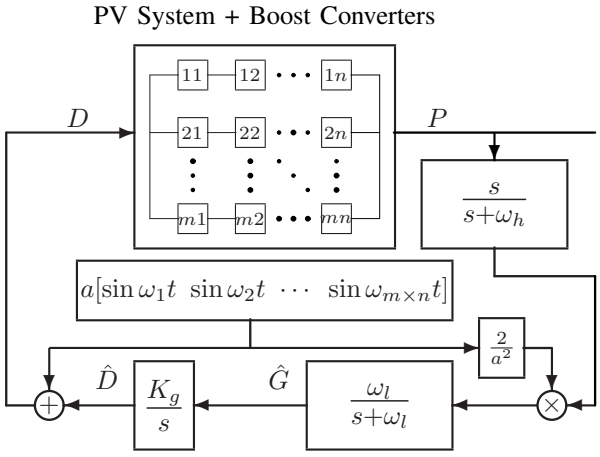

Fig. 8. Multivariable ES for MPPT of a PV system.

DC/DC converters), and "filtering" the resultant power P through the process described before. The probing frequencies ω_i's are chosen such that $\omega_i \neq \omega_j$ and $\omega_i + \omega_j \neq \omega_k$ for distinct i, j, and k. With no additional information on the Hessian (and also for simplicity), we choose the amplitudes of the probing signals to all be the same value a. As before, smallness of the probing frequencies and the matrix gain K_g are ensured by selecting these as

$$\omega_i = \omega\omega_i', \quad i \in \{1, 2, \cdots, m \times n\} \tag{14}$$

$$K_g = \omega\delta K_g' \tag{15}$$

where ω and δ are small positive constants, and ω_i' and elements of K_g' are $O(1)$ positive real parameters. The filter coefficients ω_l and ω_h are defined by (11) and (12). As before, it can be shown that for sufficiently small ω, δ, and a, and with $K_g > 0$, the estimate $\hat{D}$ of the pulse duration vector and the output P converge to $O(\omega + \delta + a)$-neighborhoods of the optimal pulse duration $D^* = [d_{11}^*\ d_{12}^*\ \cdots\ d_{mn}^*]^T$ and the MPP P^* respectively.

Parameter	Value	Unit	Parameter	Value	Unit
f_c	100	kHz	$V_{\rm dc}$	300	V
C_i	3	μF	C_o	220	μF
L	220	μH	d_0	0.5	–
K_g	$0.01I_{6\times 6}$	–	k_g	0.01	–
ω	7000	rad/s	a	0.01	–
ω_l	50	rad/s	ω_h	45	rad/s
ω_1	4500	rad/s	ω_4	5500	rad/s
ω_2	6500	rad/s	ω_5	7500	rad/s
ω_3	8500	rad/s	ω_6	9500	rad/s
m	2	–	n	3	–

TABLE I

PARAMETERS USED IN THE SIMULATIONS.

The differences between the scalar and multivariable designs become clear when one considers the update equations for the estimation error $\tilde{D} = \hat{D} - D^*$. In the multivariable case, we have

$$\dot{\tilde{D}} = K_g H \tilde{D}, \quad H := \frac{\partial^2 P}{\partial D^2}(D^*) \tag{16}$$

where H is the (negative definite) Hessian and $P = V_{dc} I_{dc}$. In the scalar ES design of Fig. 6 however, the above equation is replaced by

$$\dot{\tilde{D}} = k_g \mathcal{H} \tilde{D} \tag{17}$$

$$\mathcal{H} := \begin{bmatrix} h_{PV_{11}} & 0 & 0 & \cdots & 0 \\ 0 & h_{PV_{12}} & 0 & \cdots & 0 \\ \vdots & \vdots & \vdots & \ddots & \vdots \\ 0 & 0 & 0 & \cdots & h_{PV_{mn}} \end{bmatrix}, \tag{18}$$

where $h_{PV_{ji}} = \partial^2 P_{ji} / \partial d_{ji}^2$ and $P_{ji} = V_{ji} I_{ji}$ for all j and i (see Fig. 6), so that the equations are decoupled, and there is no way to affect the power extraction in one module by changing the pulse duration of the DC/DC converter of another module. In addition, the diagonal structure of $\mathcal{H}$ in the scalar case, coupled with the fact that this varies with irradiance, means that in the scalar design, the convergence rate of the parameters is very sensitive to partial shading, where the irradiance varies strongly from one module to another. The multivariable scheme, on the other hand, is less sensitive to the changes in the power-voltage characteristic of a specific module which results from variation of temperature or irradiance.

V. SIMULATION RESULTS

To show the effectiveness of the proposed multivariable design in Fig. 7, and compare its performance with that of the scalar design in Fig. 6, we simulate a PV system with $m = 2$ parallel strings and $n = 3$ cascade modules in each string. The PV modules are model 215N from Sanyo, with datasheet parameters presented in Section II.

Selecting all the frequencies in a narrow range creates large overshoots and steady state errors in parameter estimation. However, choosing the frequencies in a wide range causes very different convergence rates in each channel. Since we set the low-pass filter frequency equal for all the channels, the amplitude of the perturbation signal with the lowest frequency reduces less than that with the highest frequency, which in turn results in a higher feedback gain for the low frequency channel, which derives the parameter faster to the optimal value. It is possible to tune the matrix gain elements with respect to the selected frequencies. What this means is that in order to have the same convergence rate for a wide range of selected frequencies, we can choose a higher gain for higher frequencies to compensate the effect of low-pass filter. We prefer to select the frequencies in a reasonable range, between 50% up and down of the central frequency. It should be noted that central frequency should be small enough in comparison to the PWM frequency. We suggest that this be of the order of 1% of the PWM frequency. The transient for the estimate of the gradient vector contains frequencies that include harmonics of $\omega_i - \omega_j$, for all distinct i and j. The bandwidth of the low-pass filter needs to be designed with respect to these values. We suggest selecting ω_l to be of the order of 5% of the least difference between the probing frequencies. The final step is selecting the cut-off frequency of the high-pass filter, which we simply choose to be smaller than ω_l. Based on the preceding remarks, the numerical values of the design parameters are as presented in Table I.

The temperature T is assumed to be equal to 25 °C for all modules throughout. The irradiance S is assumed to be equal to 1000 W/m^2 initially, with a step change to 500 W/m^2 for modules PV$_{12}$ and PV$_{23}$ at $t = 0.5$ s and then back to 1000 W/m^2 at 1 s, so as to simulate partial shading on some modules. The output power of the entire system is shown in Fig. 9, with the estimate of the pulse duration for each module shown in Fig. 10. It is clear from Fig. 9 that the multivariable algorithm performs a uniform and faster transient against step up or step down changes in the generated power.

At the beginning all PV modules and converters have the same settings, gains, and initial conditions. Also all modules are under the same irradiance and temperature. Hence, the transient of the scalar ES for all parameters is the same as shown in Fig. 10. On the other hand, multivariable ES shows different transient for each parameter which is happening because of different frequencies of the perturbation function in each channel. The lowest frequency shows the fastest response, along with a correspondingly larger overshoot. It is possible to tune matrix K_g such that all transients look the same.

When the modules in each string are partially shaded, the overall power level decreases. The multivariable ES design recovers from this power level change faster than the scalar version. As clear from Fig. 9, the power goes to the MPP in less than half the time needed for the scalar scheme.

The irradiance level of the partially shaded modules is returned to 1000 W/m^2 at $t = 1$ s. At this point both schemes show a similar transient. It is concluded that the convergence rate of the multivariable scheme does not vary largely from step up to step down in power generation, which is not true for the scalar ES. It is clear that in the step down situation the scalar scheme shows a slower performance than the step up case.

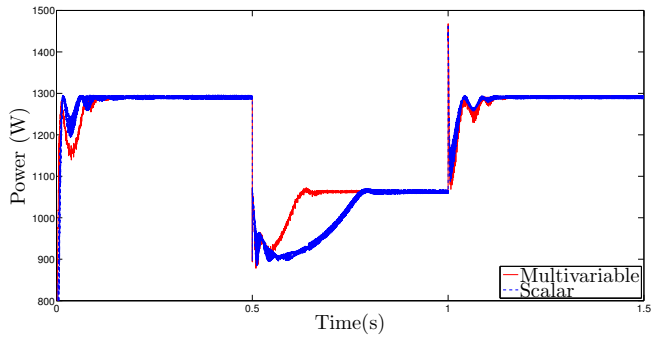

Fig. 9. Generated power in a partial shading scenario. Decentralized ES (dashed blue), and multivariable ES (solid red).

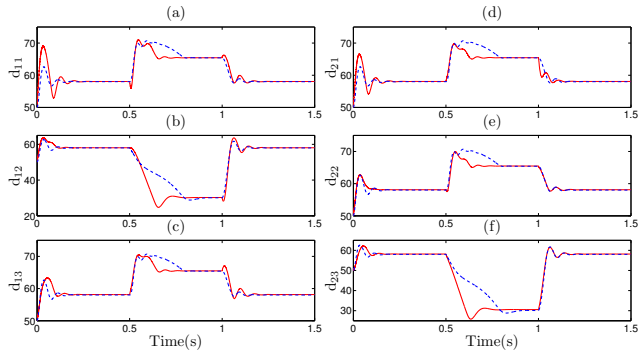

Fig. 10. Adaptation of the pulse duration. Decentralized ES (dashed blue), and multivariable ES (solid red).

VI. Conclusions

Using extremum seeking in a micro-converter configuration is a promising way to extract maximum power from a PV system. Conventionally used scalar gradient-based designs do so based on the generated power of each module. On the one hand, this requires two sensors per module, and on the other, the dependence on the level and direction of changes of the individual powers causes different transients in the parameter updates, particularly in response to sudden irradiance changes caused by partial shading. The multivariable extremum seeking design that we present removes these drawbacks. Since the Hessian of the entire system (and not individual modules) defines the performance of the parameter update, this leads to more uniform transients in response to irradiance and temperature changes, lower power ripple than the scalar design, and improved overall performance. The scheme also only uses two sensors for the overall system, resulting in lower hardware cost. The dual advantages contribute towards reduced average cost/watt, enhancing the economic viability of solar.

Acknowledgment

The second author wishes to acknowledge his gratitude to Mr. William Torre at San Diego Gas & Electric (SDG&E) Co. for getting him interested in this research, and also his encouragement and support during the two summers he spent there.

References

[1] K. Ariyur and M. Krstić, *Real-Time Optimization by Extremum Seeking Feedback*. Wiley-Interscience, 2003.

[2] A. Bratcu, I. Munteanu, S. Bacha, D. Picault, and B. Raison, "Cascaded DC-DC converter photovoltaic systems: power optimization issues," *IEEE Transactions on Industrial Electronics*, vol. 58, pp. 403–411, 2011.

[3] S. Brunton, C. Rowley, S. Kulkarni, and C. Clarkson, "Maximum power point tracking for photovoltaic optimization using ripple-based extremum seeking control," *IEEE Transactions on Power Electronics*, vol. 25, pp. 2531–2540, 2010.

[4] C. Deline, B. Marion, J. Granata, and S. Gonzalez, "A performance and economic analysis of distributed power electronics in photovoltaic systems," in *Technical Report, National Renewable Library*, 2011.

[5] S. Dhople, J. Ehlmann, A. Davoudi, and P. Chapman, "Multiple-input boost converter to minimize power losses due to partial shading in photovoltaic modules," in *Proc. of IEEE Energy Conversion Congress and Exposition (ECCE)*, 2010.

[6] T. Esram and P. Chapman, "Comparison of photovoltaic array maximum power point tracking techniques," *IEEE Transactions on Energy Conversion*, vol. 22, pp. 439–449, 2007.

[7] D. P. Hohm and M. E. Ropp, "Comparative study of maximum power point tracking algorithms," *Progress in Photovoltaics: Research and Applications*, vol. 11, p. 4762, 2003.

[8] S. Jain and V. Agarwal, "Comparison of the performance of maximum power point tracking schemes applied to single-stage grid-connected photovoltaic systems," *IET Electric Power Applications*, vol. 1, pp. 753–762, 2007.

[9] R. Kadri, J.-P. Gaubert, and G. Champenois, "An improved maximum power point tracking for photovoltaic grid-connected inverter based on voltage-oriented control," *IEEE Transactions on Industrial Electronics*, vol. 58, pp. 66–75, 2011.

[10] M. Krstić and H.-H. Wang, "Stability of extremum seeking feedback for general nonlinear dynamic systems," *Automatica*, vol. 36, pp. 595–601, 2000.

[11] P. Lei, Y. Li, Q. Chen, and J. Seem, "Extremum seeking control based integration of MPPT and degradation detection for photovoltaic arrays," in *Proc. of American Control Conference*, 2010.

[12] R. Leyva, C. Alonso, I. Queinnec, A. Cid-Pastor, D. Lagrange, and L. Martinez-Salamero, "MPPT of photovoltaic systems using extremum seeking control," *IEEE Transactions on Aerospace and Electronic Systems*, vol. 42, pp. 249–258, 2006.

[13] M. Miyatake, M. Veerachary, F. Toriumi, N. Fuji, and H. Ko, "Maximum power point tracking of multiple photovoltaic arrays: a PSO approach," *IEEE Transactions on Aerospace and Electronic Systems*, vol. 47, pp. 367–380, 2011.

[14] S. Moura and Y. Chang, "Asymptotic convergence through Lyapunov-based switching in extremum seeking with application to photovoltaic systems," in *Proc. of American Control Conference*, 2010.

[15] F.-S. Pai, R.-M. Chao, S. H. Ko, and T.-S. Lee, "Performance evaluation of parabolic prediction to maximum power point tracking for PV array," *IEEE Transactions on Sustainable Energy*, vol. 2, pp. 60–68, 2011.

[16] H. Patel and V. Agarwal, "MPPT scheme for a PV-fed single-phase single-stage grid-connected inverter operating in CCM with only one current sensor," *IEEE Transactions on Energy Conversion*, vol. 24, pp. 256–263, 2009.

[17] G. Petrone, G. Spagnuolo, and M. Vitelli, "A multivariable perturb-and-observe maximum power point tracking technique applied to a single-stage photovoltaic inverter," *IEEE Transactions on Industrial Electronics*, vol. 58, pp. 76–84, 2011.

[18] C. A. Ramos-Paja, G. Spagnuolo, G. Petrone, M. Vitelli, and J. Bastidas, "A multivariable MPPT algorithm for granular control of photovoltaic systems," in *Proc. of IEEE International Symposium on Industrial Electronics*, 2010.

[19] G. Vachtsevanos and K. Kalaitzakis, "A hybrid photovoltaic simulator for utility interactive studies," *IEEE Transactions on Energy Conversion*, vol. EC-2, pp. 227–231, 1987.

[20] H.-H. Wang and M. Krstic, "Extremum seeking for limit cycle minimization," *IEEE Transactions on Automatic Control*, vol. 45, pp. 2432–2436, 2000.

[21] H.-H. Wang, S. Yeung, and M. Krstic, "Experimental application of extremum seeking on an axial-flow compressor," *IEEE Transactions on Control Systems Technology*, vol. 8, pp. 300–309, 1999.